A hybrid numerical flux for supersonic flows with application to rocket nozzles

Advances in Aircraft and Spacecraft Science, *Vol. 7, No. 5 (2020) 387–404*
DOI: http://doi.org/10.12989/aas.2020.7.5.387

A hybrid numerical flux for supersonic flows with application to rocket nozzles

Andrea Ferrero* and Domenic D'Ambrosio

DIMEAS, Politecnico di Torino, Corso Duca degli Abruzzi 24, 10129 Torino, Italy

(Received December 30, 2019, Revised April 29, 2020, Accepted April 30, 2020)

Abstract. The numerical simulation of shock waves in supersonic flows is challenging because of several instabilities which can affect the solution. Among them, the carbuncle phenomenon can introduce nonphysical perturbations in captured shock waves. In the present work, a hybrid numerical flux is proposed for the evaluation of the convective fluxes that avoids carbuncle and keeps high-accuracy on shocks and boundary layers. In particular, the proposed flux is a combination between an upwind approximate Riemann problem solver and the Local Lax-Friedrichs scheme. A simple strategy to mix the two fluxes is proposed and tested in the framework of a discontinuous Galerkin discretisation. The approach is investigated on the subsonic flow in a channel, on the supersonic flow around a cylinder, on the supersonic flow on a flat plate and on the flow in a overexpanded rocket nozzle.

Keywords: hybrid flux; carbuncle; shock capturing; supersonic flow; discontinuous Galerkin

1. Introduction

The numerical simulation of supersonic flows represents a fundamental tool for the design of aerospace propulsion systems (rocket nozzles, transonic compressors and turbines in air breathing engines) and re-entry space vehicles. The shock waves, which can be observed in supersonic flows, introduce several numerical problems that increase the difficulty of the simulation: order of accuracy reduction, convergence problems, instabilities. Among the different numerical instabilities which can be triggered by shock waves, the carbuncle phenomenon is one of the most investigated. The carbuncle consists in the development of nonphysical distortions in the structure of the shock wave. This instability, which is observed in both 2D and 3D flows, can dramatically affect the numerical prediction of the bow shock wave in front of a re-entry vehicle or the shape of the Mach disk in an over-expanded rocket nozzle. The consequences of this numerical artefact can be quite important in several applications: for example, the maximum heat flux at which a blunt body is subjected is observed in the stagnation point but the solution in this crucial point can be significantly affected by the carbuncle.

*Corresponding author, Assistant Professor, E-mail: andrea_ferrero@polito.it

http://www.techno-press.org/?journal=aas&subpage=7 ISSN: 2287-528X(Print), 2287-5271(Online)

The carbuncle instability affects the existing numerical fluxes in different ways. A comparison of the behaviour of several numerical fluxes was reported by Pandolfi and D'Ambrosio (2001). Some upwind fluxes like the ones proposed by Osher and Solomon (1982), Pandolfi (1984) and Roe (1981) seem to be particularly prone to this instability. On the contrary, there are some other classical fluxes like the local Lax-Friedrichs or Rusanov (1962) flux, the flux vector splitting of Van Leer (1997) or the AUSM+ Liou (1996) which are immune or weakly affected from this problem. Often, the ability to avoid carbuncle is associated to large numerical dissipation as can be observed by the local Lax-Friedrichs scheme. For this reason, several efforts for the development of new carbuncle-free methods, which introduce low dissipation, have been done.
The mechanism behind the development of the carbuncle instability seems to be related to the lack of numerical dissipation in the direction tangential to the shock wave as shown by Pandolfi and D'Ambrosio (2001). In order to fix this problem, rotated numerical fluxes have been proposed. In particular, Nishikawa and Kitamura (2008) proposed a rotated flux which combines the Roe and the HLLC fluxes in order to add more dissipation in the required direction: their approach requires to solve two different Riemann problems along perpendicular directions and to combine the obtained fluxes. Jaisankar and Sheshadri (2013) proposed the Directional Diffusion Regulator for some numerical solvers of hyperbolic conservation laws with the purpose of maximise the dissipation of the numerical scheme only in the normal direction to a probable discontinuity. Wang *et al.* (2016) developed a hybrid numerical flux in which the Rusanov scheme is used near shock waves while the Roe flux is used in smooth regions. Recently, Guo and Tao (2018) proposed a hybrid AUSM+-FVS flux which combines the accuracy of the AUSM+ in boundary layers with the robustness of FVS in shock regions. An alternative strategy was proposed by Hu and Yuan (2014): they introduced a hybrid flux obtained by combining the HLLC and the FORCE scheme.
The present work describes a strategy which is similar in spirit to the approach of Hu and Yuan (2014) but uses a simpler blending method. Furthermore, in the present work the hybrid strategy will be applied by mixing the Flux Difference Splitting (FDS) approach (defined according to Pandolfi (1984) or Osher and Solomon (1982)) and the local Lax-Friedrichs or Rusanov (1962) flux. The obtained numerical flux will be used to approximate convective fluxes in the framework of a discontinuous Galerkin discretisation. However, the same numerical flux can be used in finite volume discretisations. The behaviour of the proposed method will be investigated in both viscous and inviscid supersonic flows.

2. Physical model

The test cases considered in this work are described by the 2D compressible Navier-Stokes equations or by the 2D Euler equations.The compressible Navier-Stokes equations are reported in the following:

$$\frac{\partial \rho}{\partial t} + \nabla \cdot (\rho \boldsymbol{u}) = 0 \tag{1}$$

$$\frac{\partial}{\partial t}(\rho \boldsymbol{u}) + \nabla \cdot (\rho \boldsymbol{u}\boldsymbol{u}) = -\nabla P + \nabla \cdot \boldsymbol{\tau} \tag{2}$$

$$\frac{\partial E}{\partial t} + \nabla \cdot (\boldsymbol{u}(E+P)) = \nabla \cdot (\boldsymbol{\tau} \cdot \boldsymbol{u} - \boldsymbol{q}) \tag{3}$$

where ρ, $\boldsymbol{u}$, P, E, $\boldsymbol{\tau}$, $\boldsymbol{x}$ and t are density, velocity, pressure, total energy per unit volume, viscous stresses, spatial position and time, respectively. A fluid with constant specific heat ratio γ and constant viscosity is considered. The following equation for the energy is considered:

$$E = \frac{P}{\gamma - 1} + \frac{1}{2}\rho \boldsymbol{u} \cdot \boldsymbol{u} \tag{4}$$

where γ is the specific heat ratio.
The viscous stress tensor $\boldsymbol{\tau}$ is defined as:

$$\tau_{ij} = \mu \left(\left(\frac{\partial u_i}{\partial x_j} + \frac{\partial u_j}{\partial x_i} \right) - \frac{2}{3} \frac{\partial u_k}{\partial x_k} \delta_{ij} \right) \tag{5}$$

where μ is the dynamic viscosity which is hear assumed constant.
The 2D Navier-Stokes equations can be rewritten in compact form:

$$\frac{\partial \boldsymbol{u}}{\partial t} + \nabla \cdot \boldsymbol{F} = 0 \tag{6}$$

where $\boldsymbol{u}$ is the vector of conservative variables and $\boldsymbol{F}$ contains the fluxes. The flow in the nozzle studied in Section 6.3 will be assumed axisymmetric. The 2D axisymmetric Navier-Stokes equations can be written as:

$$\frac{\partial (r\boldsymbol{u})}{\partial t} + \nabla \cdot (r\boldsymbol{F}) = r\boldsymbol{s} \tag{7}$$

where r is the radial coordinate. As a consequence of the axisymmetric assumption, the source term $\boldsymbol{s} = (0, 0, (p - \tau_{\theta\theta})/r, 0)^T$ is introduced. More details can be found in the work of Bassi *et al.* (2011). The Euler equations are obtained from the set of Equations 1-3 by neglecting the diffusive terms.

3. Numerical framework

The governing equations (Euler or Navier-Stokes equations) which describe the problems considered in this work are discretised by means of the method of lines. The spatial discretisation is performed by a second order accurate Discontinuous Galerkin (DG) method while time integration is performed with the first order explicit Euler scheme. Since steady problems are considered in this work, the steady solution is obtained by marching in time. The domain is discretised by unstructured grids with both triangular and quadrilateral elements using the Gmsh software described by Geuzaine and Remacle (2009).

The DG method is a flexible approach which allows to manage complex geometry with arbitrary discretisation order. The basic idea behind this method is related to the introduction of several degrees of freedom inside each element. In this way, the stencil of the discretisation remains compact even when high order schemes are considered: this simplified significantly the parallel implementation of the method or the management of hanging-nodes in the mesh because only the first neighbour elements are required to update the solution. Several alternatives methods have been proposed for compressible flows. Traditional ENO/WENO finite volume schemes by Liu *et al.* (1994) represent a very robust approach and they have been successfully used in several problems. However, their implementation in the presence of unstructured meshes is not trivial because of the large stencil. A comparison of several recent methods for compressible flows can be found in the books related to the ADIGMA and IDIHOM European projects, written by Kroll *et al.* (2010) and Kroll *et al.* (2015). The reader can also find a quantitative comparison of the performances of several schemes in a series of workshops devoted to high order methods, summarised by Wang *et al.* (2013).

The DG spatial discretisation is obtained by writing the governing equations in a variational form. The procedure is here described for the 2D Navier-Stokes equations but an equivalent approach should be followed for the 2D axisymmetric equations. The spatial domain Ω can be discretised with a set of elements Ω_e. The solution inside each element is described by introducing a local modal hierarchical basis. In particular a basis obtained by the orthonormalisation of a set of monomials is chosen, following the approach of Bassi *et al.* (2012): three degrees of freedom per elements ($N_e = 3$) are used in order to get a linear reconstruction with second order accuracy. The modal basis adopted for this work is built in the same way for all the elements and so the size of the basis is the same for both triangular and quadrilateral elements. The discrete solution inside each element is then expressed in terms of basis functions Φ_i and degrees of freedom $\tilde{\boldsymbol{u}}_i$:

$$\boldsymbol{u}_h(\boldsymbol{x}, t) = \sum_{i=1}^{N_e} \tilde{\boldsymbol{u}}_i \Phi_i \tag{8}$$

When the discrete solution is introduced into the conservative equation (Eq. 6) the residuals $\boldsymbol{R}_h$ are obtained:

$$\boldsymbol{R}_h = \frac{\partial \boldsymbol{u}_h}{\partial t} + \nabla \cdot \boldsymbol{F}_h \tag{9}$$

The variational formulation is obtained by setting to zero the projection of the residuals with respect to a generic function ν which belongs to the space V_h spanned by the basis functions Φ_i:

$$\int_{\Omega_e} \boldsymbol{R}_h \nu dxdy = \int_{\Omega_e} \frac{\partial \boldsymbol{u}_h}{\partial t} \nu dxdy + \int_{\Omega_e} \nabla \cdot \boldsymbol{F}_h \nu dxdy = 0 \quad \forall \nu \in V_h \tag{10}$$

Finally, integration by parts is used in order to put in evidence the fluxes $\hat{\boldsymbol{F}}_h$ across the interfaces between elements:

$$\int_{\Omega_e} \frac{\partial \boldsymbol{u}_h}{\partial t} \nu dxdy + \int_{\partial\Omega_e} (\hat{\boldsymbol{F}}_h \cdot \boldsymbol{n}) \nu ds - \int_{\Omega_e} \nabla \nu \boldsymbol{F}_h dxdy = 0 \tag{11}$$

where $\boldsymbol{n}$ is the outward-pointing unit normal vector and s is the element boundary curve. Different schemes are here considered for the computation of the convective part of the fluxes: the local Lax-Friedrichs or Rusanov (1962) flux, the Flux-Difference Splitting approach by Osher and Solomon (1982), Pandolfi (1984) or the hybrid flux proposed in this work. More details on the different schemes will be reported in the Section 5. Diffusive fluxes are evaluated by means of the Enhanced Stability Recovery method proposed by Ferrero *et al.* (2015). The solution in the presence of shock waves is stabilised through a filtering strategy following Ferrero and Larocca (2016). The flexibility of the scheme can be easily exploited in the framework of automatic adaptive approaches, in which both the size (h-adaptivity, Hartmann and Houston (2002), Remacle *et al.* (2003), Zenoni *et al.* (2017), Ferrero *et al.* (2017)), the order (p-adaptivity Burbeau and Sagaut (2005), Giorgiani *et al.* (2013), Ampellio *et al.* (2016)) or both properties (hp-adaptivity, Eskilsson (2011), Ferrero and Larocca (2017), Chalmers *et al.* (2019)) can be locally adapted following some error indicators.

The projection represented by Eq. (11) must be evaluated for all the basis functions of the elements: this gives a set of Ordinary Differential Equations in time which describes the evolution of the numerical solution:

$$\int_{\Omega_e} \sum_{i=1}^{N_e} \frac{\partial \tilde{\boldsymbol{u}}_i}{\partial t} \Phi_i \Phi_j dxdy + \int_{\partial\Omega_e} \hat{\boldsymbol{F}}_h \cdot \boldsymbol{n} \Phi_j ds - \int_{\Omega_e} \nabla\Phi_j \boldsymbol{F}_h dxdy = 0 \quad 1 \leq j \leq N_e \tag{12}$$

The Eq. 12 can be integrated with different strategies. In this work, a simple first order explicit Euler scheme is used since the considered problems are characterised by steady solutions and so the first order integrator does not influence the accuracy of the solution.

4. HLLC-FORCE Hybrid Flux

Hu and Yuan Hu and Yuan (2014) introduced a numerical flux obtained by a mix of the HLLC and FORCE fluxes in a grid aligned framework. Consider the numerical approximation of the convective fluxes for a 2D problem across a generic interface of the mesh. The flux vector is defined as $\hat{\boldsymbol{F}} = \{\hat{F}_1, \hat{F}_2, \hat{F}_3, \hat{F}_4\}^T$, where the components refer to mass, momentum in the shock normal direction, momentum in the shock tangential direction and energy. The hybrid flux proposed in Hu and Yuan (2014) is equal to the HLLC flux for the energy equation and for the momentum equation in the direction normal to the shock. In contrast, a linear combination of the two fluxes is performed for the density and momentum equation in the direction tangential to the shock. The coefficients of the combination are computed by comparing the interface normal and the shock normal which is approximated by the velocity vector jump across the interface Hu and Yuan (2014).

$$\hat{F}_1 = \omega F_1^{HLLC} + (1-\omega) F_1^{FORCE} \tag{13}$$
$$\hat{F}_2 = \omega F_2^{HLLC} \tag{14}$$
$$\hat{F}_3 = \omega F_3^{HLLC} + (1-\omega) F_3^{FORCE} \tag{15}$$

$$\hat{F}_4 = \omega F_4^{HLLC} \tag{16}$$

$$\omega = \frac{1}{2} + \frac{1}{2}\frac{\alpha_1}{\alpha_1 + \alpha_2}, \quad \alpha_1 = |\boldsymbol{n} \cdot \boldsymbol{n_s}|, \quad \alpha_2 = \sqrt{1 - \alpha_1^2} \tag{17}$$

where $\boldsymbol{n}$ is the interface normal and $\boldsymbol{n_s}$ is an estimate of the shock normal direction obtained as

$$\boldsymbol{n_s} = \begin{cases} \frac{\boldsymbol{\Delta u}}{|\boldsymbol{\Delta u}|}, & |\boldsymbol{\Delta u}| > \epsilon \\ \boldsymbol{n}, & |\boldsymbol{\Delta u}| <= \epsilon \end{cases} \tag{18}$$

where $\boldsymbol{\Delta u}$ is the velocity vector jump across the interface and ϵ is a small constant to avoid division by zero.

5. Proposed FDS-LLF Hybrid Flux

5.1 The FDS numerical flux

The FDS is based on the solution of a Riemann problem in the interface normal direction: the initial condition which defines the Riemann problem is generated by the discontinuous reconstruction at the interface that is observed in both finite volume and DG methods. The idea behind FDS is to introduce the numerical dissipation required to stabilise the scheme by following the physics of wave propagation related to the hyperbolic nature of the convective terms. The name of the scheme derives from the approach used to compute the fluxes at the interface: they are obtained by considering the flux evaluated in the left (or right) state and removing the contributions from all the waves which travel to the left (or right).
This method derives from the original Godunov (1959) work in which the flux at the interface is computed by solving exactly the Riemann problem at each interface. Since the solution can involve shock waves, the non-linear Rankine-Hugoniot relations must be used in the solution process: this requires the introduction of iterative procedures to get the exact solutions. An example of exact solution of a Riemann problem in the space-time diagram is reported in Figure 1a. Osher and Solomon (1982) and Pandolfi (1984) proposed an alternative approach in which an approximate solution of the Riemann problem is found. In particular, they avoid the use of the Rankine-Hugoniot relations by approximating the shock waves which appear in the solution with isentropic compression fans: in this way, the solution of the problem can be obtained by enforcing the conservation of the Riemann invariant between the different fields. An example of approximate solution of a Riemann problem in the space-time diagram is reported in Figure 1b.

5.2 The LLF numerical flux

The Local Lax-Friedrichs (or Rusanov) flux can be seen as a central scheme plus a dissipation term:

$$\hat{\boldsymbol{F}}^{\boldsymbol{LLF}} = \frac{\boldsymbol{F^L} + \boldsymbol{F^R}}{2} - \frac{\lambda}{2}(\boldsymbol{u_B} - \boldsymbol{u_A}) \tag{19}$$

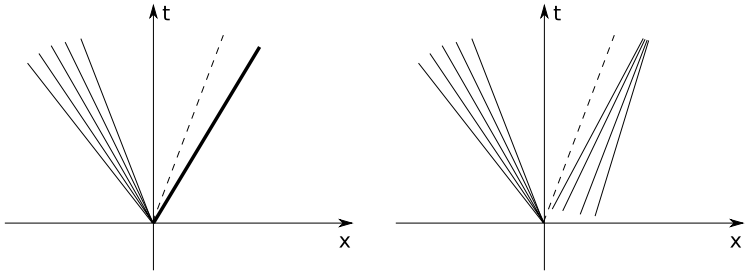

(a) (b)

Fig. 1 Exact (a) and approximate (b) solution of a Riemann problem in the interface normal direction

The first term is the average between the fluxes computed from the left ($\boldsymbol{F^L}$) and right ($\boldsymbol{F^R}$) sides while the second term contains the jump in the conservative variables ($\boldsymbol{u_B} - \boldsymbol{u_A}$) and the maximum spectral radius of the Jacobian between the two sides λ:

$$\lambda = \max\left(\tilde{u}_L + a_L, \tilde{u}_R + a_R\right) \tag{20}$$

where $\tilde{u}$ and a represent the normal velocity component and the speed of sound, respectively.

5.3 Proposed FDS-LLF Hybrid Flux

In the present work an alternative hybrid flux is proposed by introducing a linear combination of the Flux Difference Splitting (FDS) Pandolfi (1984) and the Local Lax-Friedrichs (LLF)Rusanov (1962) fluxes. The idea is to combine the accuracy of the FDS flux with the robustness of the LLF flux. While in the approach proposed by Hu and Yuan (2014) the blending of the fluxes is performed only for two equations, here the same linear combination is performed for all the components of the flux vector:

$$\hat{\boldsymbol{F}} = (1-\theta)\boldsymbol{F^{FDS}} + \theta\boldsymbol{F^{LLF}} \tag{21}$$

$$\theta = \alpha\beta \tag{22}$$

$$\alpha = \begin{cases} 1 - \frac{|\boldsymbol{\Delta u}\cdot\boldsymbol{n}|}{|\boldsymbol{\Delta u}|}, & |\boldsymbol{\Delta u}| > \epsilon \\ 0, & |\boldsymbol{\Delta u}| <= \epsilon \end{cases} \tag{23}$$

$$\beta = \min\left(\left(\frac{|\boldsymbol{\Delta u}|}{min(a_L, a_R)}\right)^{1/4}, 1\right) \tag{24}$$

where ϵ is a small constant to avoid division by zero (here set to $\epsilon = 10^{-6}$), $\boldsymbol{n}$ is the interface normal and $\boldsymbol{\Delta u}$ is the velocity vector jump across the interface. The blending function, θ, is obtained by the product between the terms α and β. The idea behind the term α is that the velocity jump direction identifies the normal to the shock wave: when the

interface is aligned to the shock wave the FDS flux should be used but when the interface is normal to the shock wave the LLF flux should be chosen. In this way, more dissipation is added in the direction tangential to the shock and carbuncle is avoided keeping a sharp shock wave profile.
A first version of the hybrid flux, which contained only the term α, was proposed at the ICNAAM 2019 conference by Ferrero and D'Ambrosio (2020). However, that version was characterised by two problems. First of all, the very dissipative LLF flux was selected for every interface in which the velocity jump vector was aligned to the interface, even in smooth regions without shock waves. Secondly, the presence of the arbitrary constant ϵ can introduce some problems when the hybrid flux is used together with an implicit time integrator based on a numerical evaluation of the Jacobian: in particular, it was observed that the perturbations used to numerically evaluate the Jacobian could trigger the switch between the LLF flux and the FDS flux, if the threshold ϵ is chosen too small. This can leads to inaccurate estimations of the derivatives which appear in the Jacobian matrix and makes difficult to perform implicit time integration. In order to avoid these two problems, the term β is introduced in the present work. This term measures the velocity jump magnitude. Since the jump at the interface between two DG elements tends to zero when the mesh is refined and the solution is smooth, this jump is a good sensor for shock waves. In this way, the term θ tends to zero in smooth regions and the FDS solver is recovered. The exponent $1/4$ which appears in Eq. 24 is introduced after some tests in order to make a compromise between the need to keep the effects of the term α in shock regions and the goal of recovering the FDS in the smooth regions. The expression in Eq. 24 contains also a max function which guarantees that the term β remains limited to 1: this is necessary to assure that a convex combination of FDS and LLF is achieved. The effects of the term β is similar to the pressure switch used by Wang *et al.* (2016) in their hybrid scheme.

The algorithm is local and can be easily implemented in both Finite Volume and Discontinuous Galerkin Finite Element codes. Since the cost of the LLF flux is significantly lower with respect to the FDS flux, the proposed hybrid approach does not increase significantly the computational cost with respect to the original FDS flux. However, the robustness is strongly improved. Furthermore, the hybrid approach does not introduce any memory overload because it works on variables which are already available from the original numerical fluxes.

6. Results

The proposed approach is tested on four different test cases and it is compared with the results provided by the FDS approach and the LLF approach. The considered test cases are characterised by compressible flows with both viscous and inviscid fluids.

6.1 Inviscid Flow in a channel with a smooth bump

This 2D test case is widely used for verification purposes and has been proposed as a benchmark in several editions of the International Workshop on High-Order CFD methods,

Table 1 L_2 entropy error convergence for channel flow

l_c/h	N_e	L_2s LLF	Order LLF	L_2s FDS	Order FDS	L_2s hybrid	Order hybrid
0.25	63	5.43E-03	-	2.59E-03	-	4.29E-03	-
0.125	247	2.86E-03	0.92	1.24E-03	1.06	1.86E-03	1.20
0.0625	966	9.86E-04	1.54	4.15E-04	1.58	5.60E-04	1.73
0.03125	3846	2.44E-04	2.02	1.05E-04	1.98	1.27E-04	2.13
0.015625	15283	4.93E-05	2.31	2.22E-05	2.25	2.46E-05	2.37

as reported by Wang *et al.* (2013). It is characterised by an inviscid flow of an ideal gas with specific heat ratio $\gamma = 1.4$ in a channel with a gaussian bump on the bottom wall. The extension of the computational domain in the horizontal direction is bounded in the interval $-1.875 \leq x/h \leq 1.875$ where h is the height of the channel at the inlet. The bottom wall is described by the equation $y/h = 0.078125e^{-25x^2}$. The inlet and the outlet are subsonic: total temperature, total pressure and inlet angle are imposed on the inlet while static pressure is imposed on the outlet. The exit static pressure corresponds to the exit Mach number $M_2 = 0.5$. Slip boundary conditions are imposed on the top and bottom walls.

The flow is studied on a sequence of unstructured grids containing both triangular and quadrilateral elements. The number of elements N_e in the different meshes is increased by reducing the characteristic length l_c of the elements. The finest mesh and the corresponding Mach field obtained by the FDS solver is reported in Figure 2.

Since this test case is characterised by an inviscid flow without shock waves the exact solution shows a constant entropy in all the domain. For this reason it is possible to quantify the discretisation error by computing the L2-norm entropy error through an integral on the domain Ω:

$$L_2s = \sqrt{\frac{\int_\Omega ((s - s_0)/c_v)^2 dxdy}{\int_\Omega dxdy}} \tag{25}$$

where s_0 is the inlet entropy which can be arbitrarily set to zero. The entropy is normalised with respect to the constant volume specific heat c_v and so the error L_2s is dimensionless. The integrals are approximated by means of the same quadrature rules used for the integration of the governing equations.

The discretisation error on the different grids is reported in Table 1. The simulations are carried out with the DG1 scheme together with the FDS solver, the LLF solver and the proposed hybrid solver. The errors in Table 1 shows that all the solvers tend to the theoretical convergence order as the mesh is refined. This is shown also by the plot in Figure 3 which allows to compare the slopes obtained by the convergence analysis referred to the different solvers. This preliminary test shows that the FDS and the hybrid solvers produce an error which is systematically lower with respect to the LLF solver: this motivates the introduction of the hybridisation procedure which aims to avoid the use of the LLF solver where there is no risk of carbuncle.

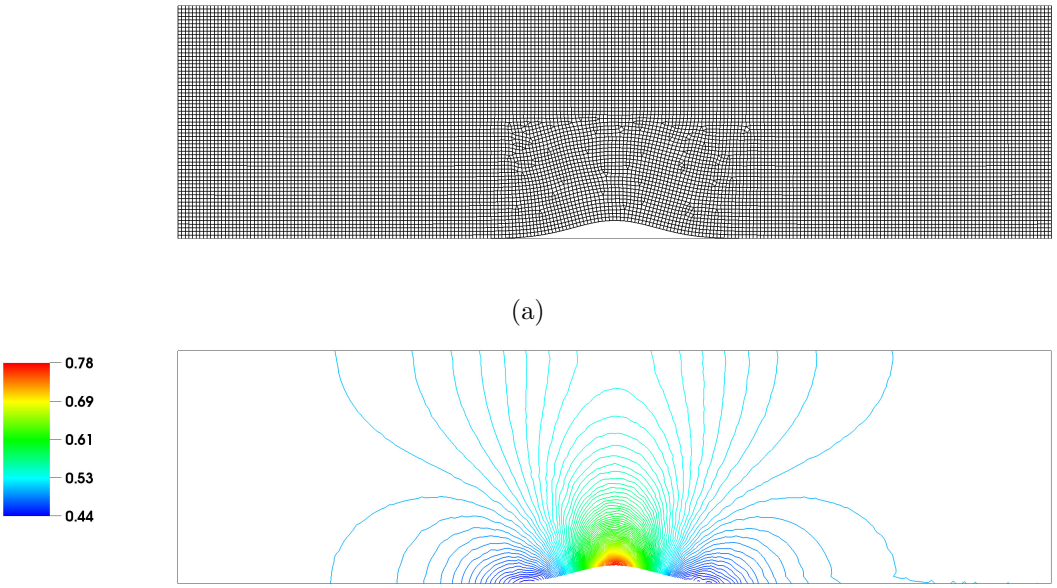

(a)

(b)

Fig. 2 Finest mesh (a) and Mach field (b) in the channel with bump (DG1 with FDS on finest mesh)

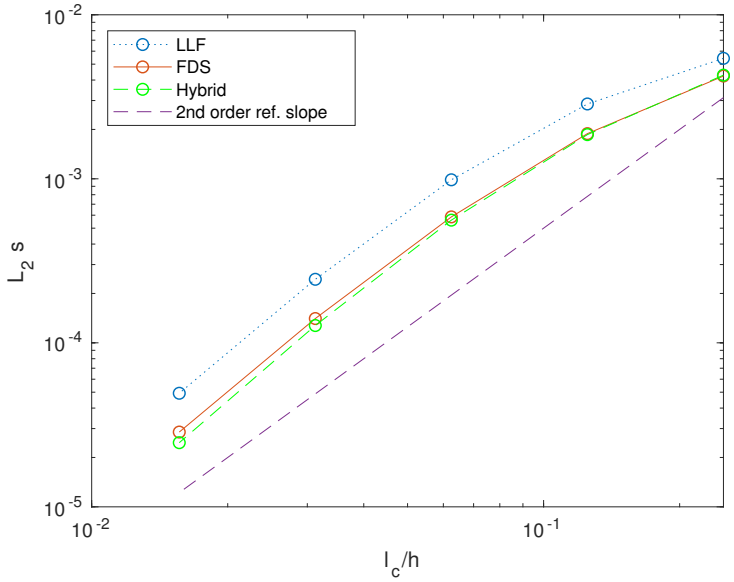

Fig. 3 L_2 entropy error convergence for channel flow with different solvers

6.2 Inviscid Supersonic Flow Around a Cylinder at Mach=4

The 2D supersonic inviscid flow around a circular cylinder at Mach=4 is simulated with a second order accurate DG scheme. An ideal gas with specific heat ratio $\gamma = 1.2$ is considered. The computational domain is discretised by means of a structured mesh with 160×80 elements reported in Figure 4a. In order to understand the behaviour of the hybrid scheme the element-averaged θ variable is reported in Figure 4b. The average is performed element-wise by considering the values assumed by θ on all the interfaces of a given element. The plot shows that the FDS scheme is used in most of the domain and the hybridisation is activated mainly in the shock region. The Mach field is reported in Figure 5 where the FDS, the proposed hybrid scheme and the LLF scheme are compared. The FDS scheme shows a significant distortion of the shock profile on the symmetry axis due to the carbuncle instability. This error influences all the subsonic region close to the stagnation point. On the contrary, the LLF scheme does not show any sign of carbuncle but it shows poor resolution on the shockwave. The proposed hybrid scheme keeps the good resolution of the FDS scheme without developing the carbuncle instability.

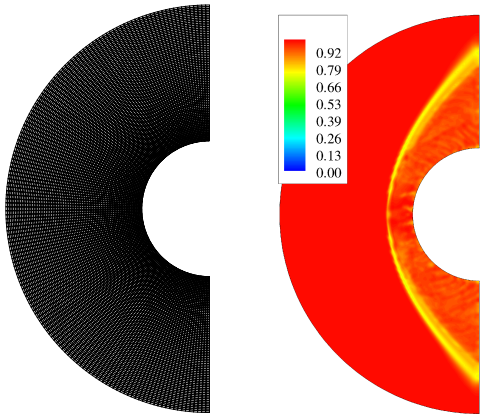

(a) (b)

Fig. 4 Computational mesh (a) and element-averaged θ field (b) for supersonic flow around a circular cylinder

6.3 Over-expanded rocket nozzle flow

The inviscid flow in a axisymmetric converging-diverging nozzle with an area expansion ratio $\epsilon_A = 80$ is studied. The domain is discretised with an unstructured mesh with both quadrilateral and triangular elements (22651 elements) reported in Figure 6a. The Frontal-Delaunay for quads algorithm is employed and an attractor to refine the mesh in the shock region is introduced. Far field boundary conditions are employed for the external boundaries which are located at a distance equal to 100 throat diameters from the nozzle exit. The 2D axisymmetric Euler equations are solved. The Nozzle Pressure Ratio (NPR, given by the ratio from the inlet total pressure and the ambient static pressure) is set to 121. The fluid is assumed to be an ideal gas with specific heat ratio $\gamma = 1.2$. In these conditions, the

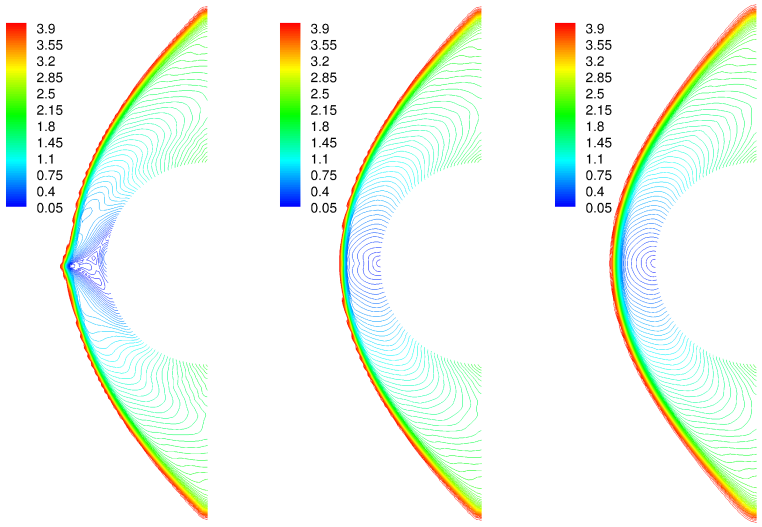

(a) (b) (c)

Fig. 5 Mach field around a cylinder at $M_\infty = 4$: (a) FDS flux, (b) proposed hybrid flux, (c) LLF flux

nozzle is strongly over-expanded and a shock wave system with a central Mach disk appears at the exit. Figure 7 shows the predicted Mach field with the FDS scheme, the proposed hybrid approach and the LLF scheme. A comparison between the results in the Mach disk region confirms the behaviour observed in the previous test case: while the FDS scheme is affected by the carbuncle instability, the LLF scheme is immune to this problem but has poor resolution on the shock wave. The proposed hybrid scheme is again able to avoid the carbuncle while keeping good resolution on the shock. This is particularly evident on the internal oblique shock wave which is weakly noticeable in the LLF solution while it is clearly visible in the hybrid solution. The Figure 6b reports the element-averaged θ field which shows that the FDS scheme is used in most of the domain.

6.4 Flat Plate Boundary Layer at $M_\infty = 5$

Finally, the 2D viscous flow on a flat plate is studied in order to evaluate the behaviour of the proposed method in the presence of boundary layers. The test case is characterised by a supersonic flow ($M_\infty = 5$) of air ($\gamma = 1.4$, $Pr = 0.72$) on a isothermal plate ($T_w = T_\infty = 72K$). The mesh is structured and contains 160×100 elements. The growing factor in the wall normal direction is equal to 1.02. A picture of the mesh is reported in Figure 8a. The Mach field with the three numerical fluxes is shown in Figure 9: the plot shows that the FDS and the hybrid schemes gives almost equivalent results while the LLF scheme tends to smear the oblique shock wave generated from the leading edge. The plot in Figure 8b shows that the FDS is adopted everywhere with the exception of the shock region and a small layer close to the wall. The pressure distribution as a function of the wall distance (y) normalised with respect to the plate length (L) is reported in Figure 10 for a station with a local Reynolds number $Re_x = 55625$. The plot shows clearly the better resolution obtained by the FDS

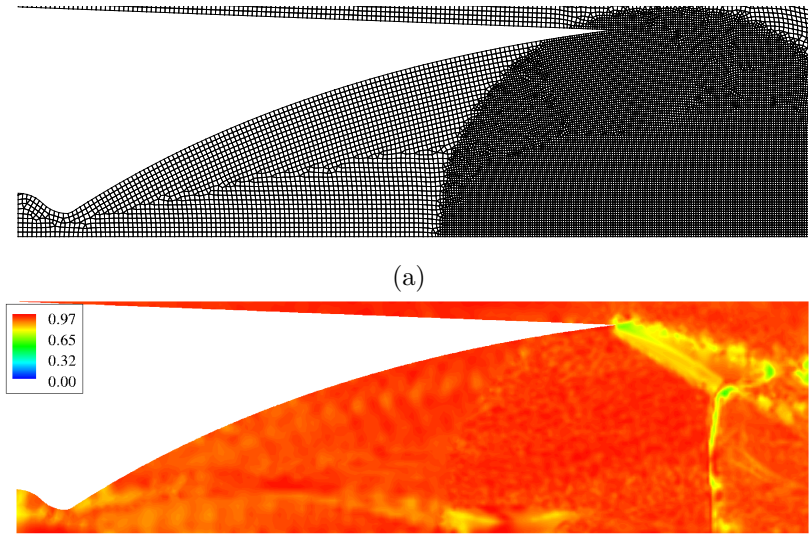

(a)

(b)

Fig. 6 Computational mesh (a) and element-averaged θ field (b) for nozzle flow

and hybrid schemes on the shock with respect to the LLF scheme. In particular, the results are in line with the reference solution published byPandolfi and D'Ambrosio (2002). Both the LLF and the hybrid scheme present some oscillations close to wall. This problem, which affects the LLF scheme in present numerical framework, is inherited by the hybrid scheme since it tends to LLF in a small layer of cells close to wall, as shown by Figure 8b. Future investigations will be devoted to substitute the LLF scheme with an alternative dissipative and carbuncle-free scheme.

7. Conclusions

In this work a hybrid numerical scheme for the computation of convective fluxes is proposed in a DG framework. The scheme is based on a convex combination of two existing schemes: the FDS scheme (which is very accurate but affected by the carbuncle instability) and the LLF scheme (which is very dissipative but carbuncle free). The basic idea of the proposed approach is to perform a scalar product between the interface normal and the velocity vector jump across the interface: in this way it is possible to apply the FDS scheme in the direction normal to the shock wave while the LLF scheme is used in the tangential direction. This makes it possible to achieve the better properties of both schemes: shock capturing with sharp resolution without the carbuncle instability. Furthermore, the switch function is augmented by a sensor based on the velocity jump magnitude with the purpose of avoiding numerical clipping from one scheme to the other in smooth regions. This sensor also helps in avoiding the use of the LLF scheme far from shock waves.
The behaviour of the proposed scheme is investigated on the inviscid subsonic flow in a channel, on the inviscid supersonic flow around a circular cylinder, on an overexpanded rocket

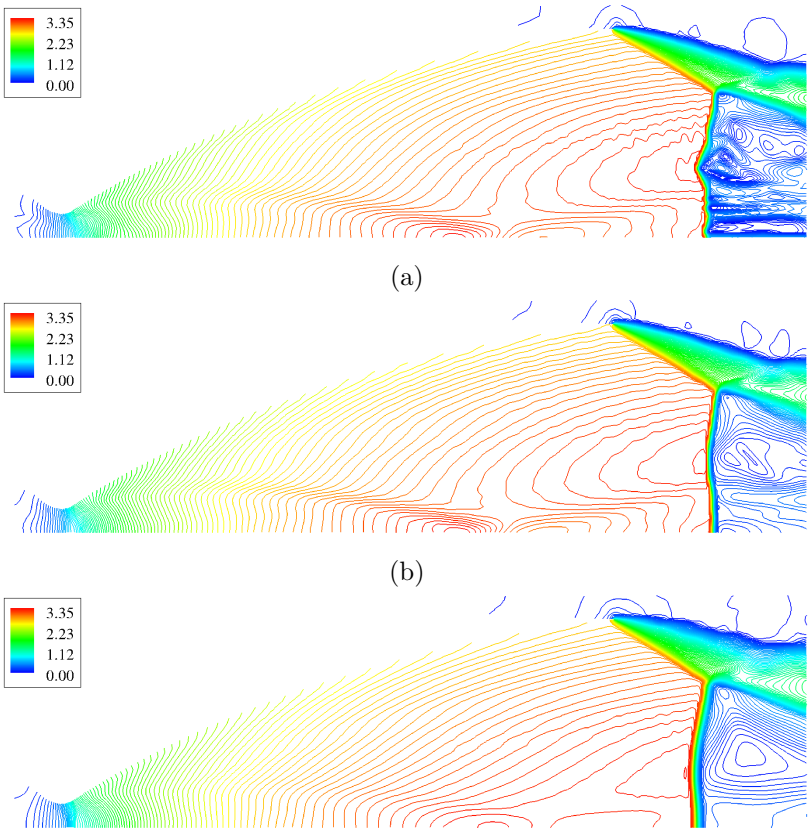

Fig. 7 Mach field in overexpanded nozzle with FDS scheme (a), proposed hybrid scheme (b) and LLF scheme (c)

nozzle flow and on the supersonic viscous flow on a flat plate. The results appear promising in terms of accuracy and carbuncle prevention with a small increase of the computational cost with respect to the FDS scheme. The proposed approach, as the original FDS and LLF schemes, can be applied on both finite volume methods and discontinuous Galerkin methods.

Acknowledgements

Computational resources were provided by HPC@POLITO, a project of Academic Computing within the Department of Control and Computer Engineering at the Politecnico di Torino (http://www.hpc.polito.it).

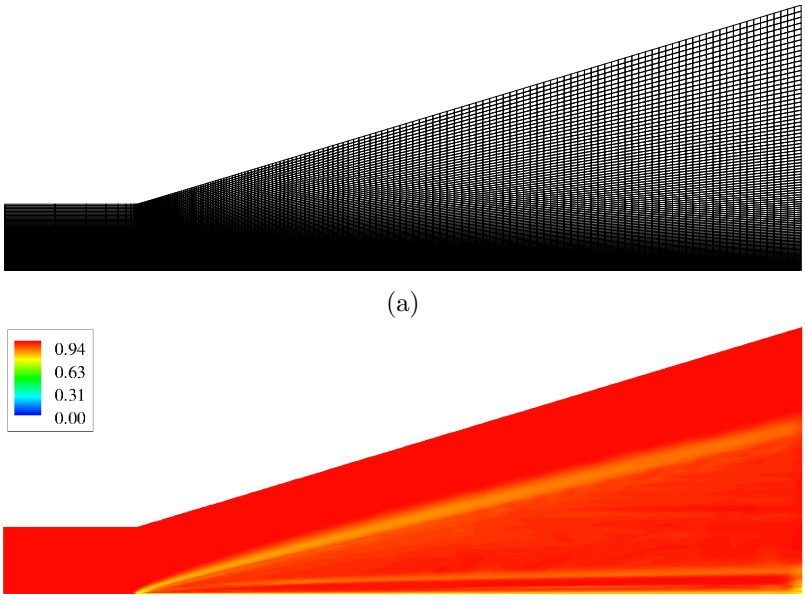

(a)

(b)

Fig. 8 Computational mesh (a) and element-averaged θ field (b) for supersonic flow over a flat plate

References

Ampellio, E., Bertini, F., Ferrero, A., Larocca, F. and Vassio, L. (2016), "Turbomachinery design by a swarm-based optimization method coupled with a CFD solver", *Adv. Aircraft Spacecraft Sci.*, **3**(2), 149, https://doi.org/10.12989/aas.2016.3.2.149.

Bassi, F., Botti, L., Colombo, A., Di Pietro, D.A. and Tesini, P. (2012), "On the flexibility of agglomeration based physical space discontinuous Galerkin discretizations", *J. Comput. Phys.*, **231**(1), 45–65, https://doi.org/10.1016/j.jcp.2011.08.018.

Bassi, F., Cecchi, F., Franchina, N., Rebay, S. and Savini, M. (2011), "High-order discontinuous Galerkin computation of axisymmetric transonic flows in safety relief valves", *Comput. Fluids*, **49**(1), 203–213, https://doi.org/10.1016/j.compfluid.2011.05.015.

Burbeau, A. and Sagaut, P. (2005), "A dynamic p-adaptive discontinuous Galerkin method for viscous flow with shocks", *Comput. Fluids*, **34**(4-5), 401–417, https://doi.org/10.1016/j.compfluid.2003.04.002.

Chalmers, N., Agbaglah, G., Chrust, M. and Mavriplis, C. (2019), "A parallel hp-adaptive high order discontinuous Galerkin method for the incompressible Navier-Stokes equations", *J. Comput. Phys. X*, **2**, 100023, https://doi.org/10.1016/j.jcpx.2019.100023.

Eskilsson, C. (2011), "An hp-adaptive discontinuous Galerkin method for shallow water flows", *Int. J. Numer. Methods Fluids*, **67**(11), 1605–1623, https://doi.org/10.1002/fld.2434.

Ferrero, A. and D'Ambrosio, D. (2020), "An Hybrid Numerical Flux for Supersonic Flows with Application to Rocket Nozzles", in "17-th International Conference of Numerical Analysis and Applied Mathematics", AIP Conference Proceedings.

Ferrero, A. and Larocca, F. (2016), "Feedback filtering in discontinuous Galerkin methods for Euler equations", *Prog. Comput. Fluid Dyn.*, **16**(1), 14–25, https://doi.org/10.1504/PCFD.2016.074221.

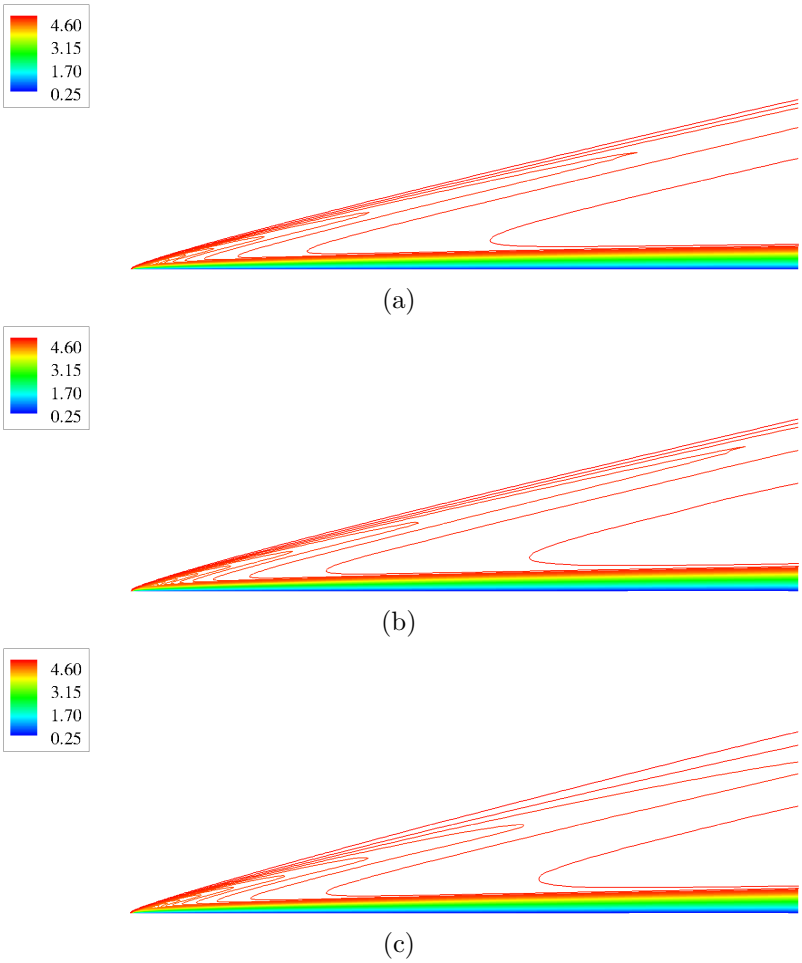

Fig. 9 Mach field in supersonic flow over a flat plate with FDS scheme (a), proposed hybrid scheme (b) and LLF scheme (c)

Ferrero, A. and Larocca, F. (2017), "Adaptive CFD schemes for aerospace propulsion", in "J. Phys. Conf. Ser.", volume 841, page 012017, IOP Publishing, https://doi.org/10.1088/1742-6596/841/1/012017.

Ferrero, A., Larocca, F. and Bernaschek, V. (2017), "Unstructured discretisation of a non-local transition model for turbomachinery flows", *Adv. Aircraft Spacecraft Sci.*, **4**(5), 555–571, https://doi.org/10.12989/aas.2017.4.5.555.

Ferrero, A., Larocca, F. and Puppo, G. (2015), "A robust and adaptive recovery-based discontinuous Galerkin method for the numerical solution of convection–diffusion equations", *Int. J. Numer. Methods Fluids*, **77**(2), 63–91, https://doi.org/10.1002/fld.3972.

Geuzaine, C. and Remacle, J.F. (2009), "Gmsh: A 3-D finite element mesh generator with built-in pre-and post-processing facilities", *Int. J. Numer. Methods Eng.*, **79**(11), 1309–1331, https://doi.org/10.1002/nme.2579.

Giorgiani, G., Fernández-Méndez, S. and Huerta, A. (2013), "Hybridizable discontinuous Galerkin

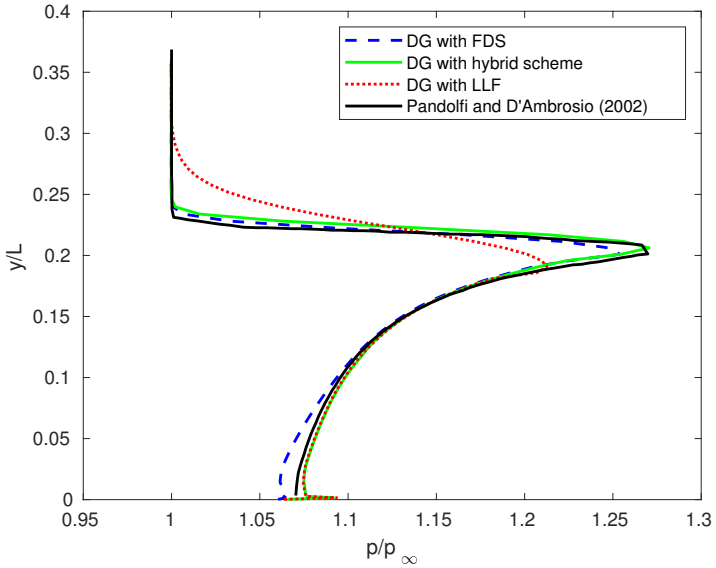

Fig. 10 Pressure distribution in a boundary layer at $M_\infty = 5$, $Re_x = 55625$

p-adaptivity for wave propagation problems", *Int. J. Numer. Methods Fluids*, **72**(12), 1244–1262, https://doi.org/10.1002/fld.3784.

Godunov, S.K. (1959), "A difference scheme for numerical solution of discontinuous solution of hydrodynamic equations", *Math. Sbornik*, **47**, 271–306.

Guo, S. and Tao, W.Q. (2018), "A hybrid flux splitting method for compressible flow", *Numer. Heat Tr. B-Fund.*, **73**(1), 33–47, https://doi.org/10.1080/10407790.2017.1420315.

Hartmann, R. and Houston, P. (2002), "Adaptive discontinuous Galerkin finite element methods for the compressible Euler equations", *J. Comput. Phys.*, **183**(2), 508–532, https://doi.org/10.1006/jcph.2002.7206.

Hu, L.J. and Yuan, L. (2014), "A Robust Hybrid HLLC-FORCE Scheme for Curing Numerical Shock Instability", in "Applied Mechanics and Materials", volume 577, pages 749–753, Trans Tech Publ, https://doi.org/10.4028/www.scientific.net/AMM.577.749.

Jaisankar, S. and Sheshadri, T. (2013), "Directional Diffusion Regulator (DDR) for some numerical solvers of hyperbolic conservation laws", *J. Comput. Phys.*, **233**, 83–99, https://doi.org/10.1016/j.jcp.2012.07.031.

Kroll, N., Bieler, H., Deconinck, H., Couaillier, V., van der Ven, H. and Sorensen, K. (2010), *ADIGMA–A European Initiative on the Development of Adaptive Higher-Order Variational Methods for Aerospace Applications: Results of a Collaborative Research Project Funded by the European Union, 2006-2009*, volume 113, Springer Science & Business Media, https://doi.org/10.1007/978-3-642-03707-8.

Kroll, N., Hirsch, C., Bassi, F., Johnston, C. and Hillewaert, K. (2015), *IDIHOM: Industrialization of High-Order Methods-A Top-Down Approach: Results of a Collaborative Research Project Funded by the European Union, 2010-2014*, volume 128, Springer, https://doi.org/10.1007/978-3-319-12886-3.

Liou, M.S. (1996), "A sequel to ausm: Ausm+", *J. Comput. Phys.*, **129**(2), 364–382, https://doi.org/10.1006/jcph.1996.0256.

Liu, X.D., Osher, S. and Chan, T. (1994), "Weighted essentially non-oscillatory schemes", *J. Comput. Phys.*, **115**(1), 200–212, https://doi.org/10.1006/jcph.1994.1187.

Nishikawa, H. and Kitamura, K. (2008), "Very simple, carbuncle-free, boundary-layer-resolving, rotated-hybrid Riemann solvers", *J. Comput. Phys.*, **227**(4), 2560–2581, https://doi.org/10.1016/j.jcp.2007.11.003.

Osher, S. and Solomon, F. (1982), "Upwind difference schemes for hyperbolic systems of conservation laws", *Math. Comput.*, **38**(158), 339–374, https://doi.org/10.1090/S0025-5718-1982-0645656-0.

Pandolfi, M. (1984), "A contribution to the numerical prediction of unsteady flows", *AIAA J.*, **22**(5), 602–610, https://doi.org/10.2514/3.48491.

Pandolfi, M. and D'Ambrosio, D. (2001), "Numerical instabilities in upwind methods: analysis and cures for the carbuncle phenomenon", *J. Comput. Phys.*, **166**(2), 271–301, https://doi.org/10.1006/jcph.2000.6652.

Pandolfi, M. and D'Ambrosio, D. (2002), "Performances of upwind methods in predicting shear-like flows", *Comput. Fluids*, **31**(4-7), 725–744, https://doi.org/10.1016/S0045-7930(01)00071-8.

Remacle, J.F., Flaherty, J.E. and Shephard, M.S. (2003), "An adaptive discontinuous Galerkin technique with an orthogonal basis applied to compressible flow problems", *SIAM Rev.*, **45**(1), 53–72, https://doi.org/10.1137/S00361445023830.

Roe, P.L. (1981), "Approximate Riemann solvers, parameter vectors, and difference schemes", *J. Comput. Phys.*, **43**(2), 357–372, https://doi.org/10.1016/0021-9991(81)90128-5.

Rusanov, V.V. (1962), "The calculation of the interaction of non-stationary shock waves and obstacles", *USSR Comput. Math. Math. Phys.*, **1**(2), 304–320, https://doi.org/10.1016/0041-5553(62)90062-9.

Van Leer, B. (1997), "Flux-vector splitting for the Euler equation", in "Upwind and High-Resolution Schemes", pages 80–89, Springer, https://doi.org/10.1007/978-3-642-60543-7_5.

Wang, D., Deng, X., Wang, G. and Dong, Y. (2016), "Developing a hybrid flux function suitable for hypersonic flow simulation with high-order methods", *Int. J. Numer. Methods Fluids*, **81**(5), 309–327, https://doi.org/10.1002/fld.4186.

Wang, Z.J., Fidkowski, K., Abgrall, R., Bassi, F., Caraeni, D., Cary, A., Deconinck, H., Hartmann, R., Hillewaert, K., Huynh, H.T. *et al.* (2013), "High-order CFD methods: current status and perspective", *Int. J. Numer. Methods Fluids*, **72**(8), 811–845, https://doi.org/10.1002/fld.3767.

Zenoni, G., Leicht, T., Colombo, A. and Botti, L. (2017), "An agglomeration-based adaptive discontinuous Galerkin method for compressible flows", *Int. J. Numer. Methods Fluids*, **85**(8), 465–483, https://doi.org/10.1002/fld.4390.

CC